5. A Detailed Characterization of Dansgaard-Oeschger Cycles at Site 1063 (Bermuda Rise)[1]

G.B. Dunbar[2]

ABSTRACT

Dansgaard-Oeschger (D-O) cycles in sediment at Site 1063 are characterized by distinct fluctuations in physical properties. Stadials are marked by low bulk density and interstadials by high bulk density. Compressional (*P-*)wave velocity is in phase with bulk density over some but not all depth intervals. Four of the D-O cycles straddling the oxygen isotope Stage 4/5 boundary have been studied in detail to understand the origin of the physical properties changes. Sediment on the Bermuda Rise is comprised of three main components: calcite, aluminosilicate minerals, and biogenic silica. Calcite concentrations vary from 1% to 43% of bulk sediment and are highest during interstadials. Aluminosilicate concentrations vary from 52% to 92% of bulk sediment and are highest during stadials. The major element ratios Al_2O_3/TiO_2 and K_2O/Al_2O_3 show increases across bulk density cycles, suggesting a change in the composition of aluminosilicates. This interpretation is supported by mineralogical analyses, which show a subtle change in clay composition. Biogenic silica concentrations vary from 0% to 23% of bulk sediment and are also highest during stadials. However, the abundance of silica varies significantly from one D-O cycle to another. Silt and fine sand abundance also increase during the first of the four stadials. This coarsening of sediment coincides with the increase in biogenic silica. The low grain density and high porosity associated with biogenic silica result in intervals of low bulk-sediment density. The abundance of biogenic silica closely matches *P*-wave velocity, suggesting that silica imparts a greater rigidity to the sediment.

[2]School of Earth Sciences, James Cook University, Qld 4811, Australia. (Present address: Antarctic Research Centre, Victoria University of Wellington, PO Box 600, Wellington New Zealand)
gavin.dunbar@vuw.ac.nz

INTRODUCTION

Major reorganizations of North Atlantic circulation have occurred in the past on the millennial time scale. These oceanographic changes, termed Dansgaard-Oeschger (D-O) cycles, are particularly evident in the sedimentary record as color changes in sediment deposited rapidly during oxygen isotope Stages 3 through 5 (Dansgaard et al., 1993; Bond et al., 1993). The color change is partly linked to variations in carbonate and hematite content (e.g., Barranco et al. 1989; Keigwin and Jones 1994; Adkins et al. 1997).

The Bermuda Rise is located in the northwest Atlantic Ocean approximately 1000 km from the continental margin of the eastern United States (Fig. F1). The rise is a depocenter for sediment redistributed from elsewhere (e.g., Biscaye and Eittreim, 1977; Laine and Hollister, 1981). Such sediment focusing has resulted in linear sedimentation rates up to 100 times the open-ocean average, allowing high-frequency changes in sediment composition to be preserved. Previous workers (Keigwin and Jones, 1989; Adkins et al., 1997) have shown that sub-Milankovitch variations in grayscale and $CaCO_3$ content related to D-O cycles are evident in Bermuda Rise sediments.

Site 1063 was drilled on the Bermuda Rise during Leg 172 (Fig. F1). The upper 35 m of sediment at this location shows high-frequency cycles in *P*-wave velocity and bulk density apparently related to D-O cycles (Fig. F2A) (Keigwin, Rio, Acton, et al., 1998). However, an intriguing observation is that *P*-wave velocity is at times in phase and at times out of phase with bulk density (Fig. F2A). These physical properties changes are not consistent with simple variations in carbonate content as the physical cause for D-O cycles in sediment. The purpose of this paper is to determine the physical cause of D-O cycles in sediment at Site 1063.

METHODS

X-Ray Diffraction

Thirty-one bulk sediment samples between 25.38 and 29.49 meters below seafloor (mbsf) were collected from Site 1063. The sampling interval is typically 0.1 m but in some cases is up to 0.5 m. These bulk samples were oven dried at 105°C for at least 24–36 hr to remove pore water. Approximately 2 g of each sample was crushed and homogenized for 10 s in a Rocklabs mini-mill with a tungsten carbide mill head and holder. A small amount of sample (~0.1 g) was smeared onto a glass disc using distilled water and subsequently dried. Care was taken to ensure the glass disc was completely covered with sample.

All crushed and homogenized samples were analyzed for mineralogy using a Siemens D-5000 X-ray diffractometer at the James Cook University Advanced Analytical Centre (JCU-AAC). The diffractometer was fitted with a copper tube, slit system, and postsample graphite monochromator. All samples were run at 40 kV and 30 mA and from 1.3°2θ to 65°2θ at 0.5°2θ per minute. Sample holders were rotated during analyses to minimize preferred orientation.

Quantification of the resulting X-ray diffraction (XRD) data was by means of a "Rietveld" synthesis using the software package Siroquant, which quantifies the phases present by fitting a synthetic XRD profile to the observed pattern (Taylor, 1991). The synthetic profile is calcu-

F1. Location of Site 1063 on the Bermuda Rise in the northwest Atlantic Ocean, p. 9.
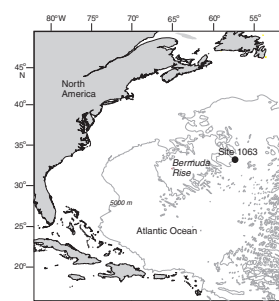
F2. Physical properties records at Hole 1063D, p. 10.
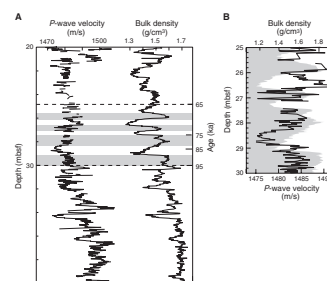
lated by constructing diffraction patterns for each phase thought to be present in the sample from the respective fundamental crystal structure data.

Amorphous (biogenic) silica was quantified using a modified cristobalite diffraction model, whereby the cristobalite peak width parameter (*w*) was empirically modified to fit the degree of crystallinity evident in the diffraction pattern. The accuracy of this method to estimate silica was assessed by quantifying known mixtures of chromatography grade silica gel and quartz. Four quartz and silica gel mixtures were crushed and homogenized for 10 s in a tungsten carbide ring mill and smeared on glass discs. Care was taken to ensure the glass disc was completely covered. Results of these analyses of quartz-silica gel mixtures are given in Table T1. As silica gel may have different spectral properties from biogenic silica, it is unclear whether this accuracy applies to estimations of the abundance of biogenic silica in samples from Site 1063. However, the amount of biogenic silica in any given sample can be constrained from concentrations of major element oxides (see below).

X-Ray Fluorescence

Small (1–2 g) splits of the bulk samples dried and crushed for XRD analyses were analyzed for major element oxide concentrations by X-ray fluorescence (XRF). Powdered samples were roasted at 1000°C for about 14 hr. Approximately 0.6 g of each roasted powder was then mixed with Norrish Hutton XRF flux and fused into a glass disc. Major element oxide concentrations were obtained using a Siemens SRS-3000 XRF spectrometer at JCU-AAC by comparison to concentration curves defined by analyses of 15 geological standards. Repeated analyses of multiple pressed glass discs of a common geological standard (AGV-1) each have concentrations of all major element oxides to within 2% of certified values (Gladney et al., 1992).
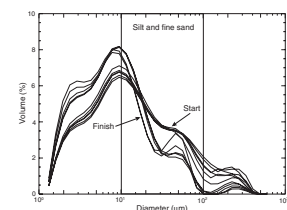
Particle Size

Particle size was determined on selected bulk samples between 25.8 and 27.2 mbsf. The chosen depth interval corresponds to a zone of low bulk density and high *P*-wave velocity. All of these samples were examined with a Malvern Mastersizer X laser particle size analyzer in the James Cook University Marine Geophysical Laboratory (e.g., Woolfe et al., 1998). Use of this instrument involves adding suspended sediment to a sample chamber, which is then pumped via a recirculating system through a narrow glass cell of 18 mm diameter and 2.4 mm width. As particles pass through the cell they induce forward scattering of a He-Ne laser beam. Particle size is quantified from the diffraction of the laser beam.

Two procedures for preparing samples were used for determining particle size. Samples were initially disaggregated using an ultrasonic probe on the Mastersizer particle size analyzer. However, repeated measurements of a single sample over time indicated that a stable size distribution could not be reached for Bermuda Rise sediment using this method (Fig. F3). In particular, the amount of sediment between 10 and 200 µm decreases over time. Thus, an alternative procedure was followed. Approximately 0.6 g of wet sediment was suspended in 40 mL of distilled water in a screw cap container. The containers were placed inside a rotating cylinder for 12 hr to gently agitate the sediment. Repeated analy-

ses of the same sample shows that results are reproducible with the same sample preparation (Fig. F4).

RESULTS

Bulk Mineralogy

As determined by XRD, sediment on the Bermuda Rise is comprised of three basic components (Table T2): calcite (1%–43%), aluminosilicates (52%–92%), and amorphous silica (0%-23%). Aluminosilicate minerals are dominated by quartz, illite-type clays, and Na- and K-feldspars. Minor phases (<10%) include Ca-feldspar, dolomite, chlorite, kaolinite, muscovite, and halite. The small amount of halite probably precipitated from pore water during drying. Shipboard smear slide analyses show that the amorphous silica is of biogenic origin. Interestingly, some of this silica may be transported from shallow depths to the Bermuda Rise rather than produced in the overlying water column (D. Winter, pers. comm., 1999).

Physical properties changes over the studied sediment interval correspond to changes in mineralogy (Fig. F5). Intervals of high bulk density are marked by high concentrations of calcite (Fig. F5A). Conversely, intervals of low bulk density correspond to high concentrations of aluminosilicate minerals (Fig. F5C). Intervals of high P-wave velocity and low bulk density relate to high concentration of biogenic silica (Figs. F5C, F5D, F5E).

Carbonate and biogenic silica typically serve as a dilutant in marine sediment. Thus, the various aluminosilicate phases were examined by recalculating their abundance on a calcite- and biogenic silica–free basis. In general, the relative proportions of quartz, feldspars, and clay are fairly constant downcore. The exceptions are muscovite, which is generally more abundant over intervals of low bulk density, and illite-type clays, which are generally more abundant during periods of high bulk density (Fig. F5G).

Bulk Chemistry

Bulk sediment from the Bermuda Rise shows a wide range in major element oxide compositions (Table T3), although this range is less than that determined for core-top samples across the entire northwest Atlantic (Ericson et al., 1961) (Fig. F6). Much of the chemical variation is caused by differences in the abundance of calcite ($CaCO_3$). As evident by the strong correlation between CaO and calcite (Fig. F7), calcium is hosted almost entirely in calcite. When this carbonate dilution effect is removed, SiO_2, TiO_2, Al_2O_3, and K_2O concentrations vary within the relatively narrow ranges of 42%–56%, 0.57%–0.73%, 12.0%–15.4%, and 1.1%–3.4%, respectively. However, in spite of carbonate dilution, several downcore trends in major elements are evident. Of particular interest is that the Al_2O_3/TiO_2 and K_2O/Al_2O_3 ratios show excellent correlations with downcore variations in bulk density (Figs. F5E, F5F). The SiO_2/Al_2O_3 ratio also shows correlations with P-wave velocity and the abundance of biogenic silica determined by XRD (Fig. F5C).

Major element oxide concentrations can be used to assess mineralogical compositions determined by XRD. The expected total SiO_2, Al_2O_3, and CaO concentrations for each sample were calculated by multiplying the abundance of each mineral phase by the weight percent of Si,

F4. Reproducibility of particle size analysis on different sample aliquots after gentle agitation without ultrasound, p. 12.
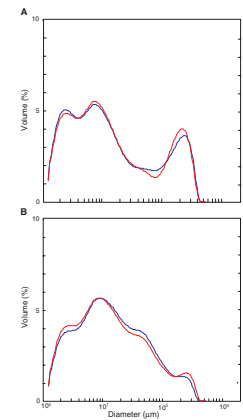
T2. Mineralogical composition of bulk sediment from Hole 1063D determined by XRD, p. 21.

F5. Downcore trends in mineralogy and chemistry compared to bulk density, p. 13.
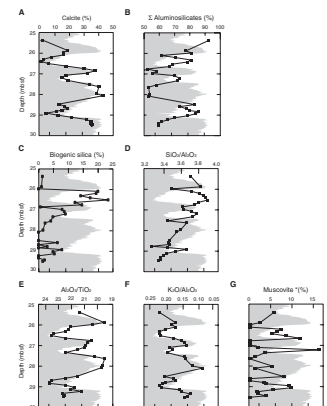
T3. Chemical composition of the bulk sediment from Hole 1063D determined by XRF, p. 22.

Al, and Ca contained in each phase (Table T4). For example, albite (NaAlSi$_3$O$_8$) constitutes 20% of Sample 172-1063D-4H-3, 108–109 cm, at 25.38 mbsf. Thus, albite contributes 13.5%, 3.8%, and 0% of the total SiO$_2$, Al$_2$O$_3$, and CaO concentrations, respectively, in the bulk sample. The sum of calculated SiO$_2$, Al$_2$O$_3$, and CaO concentrations for all minerals renders expected total oxide concentrations. The mean difference for SiO$_2$ determined by XRD and XRF is 6.6% with a standard deviation of 3.1%; similarly, the difference for Al$_2$O$_3$ is 0.5% with a standard deviation of 1.0%, and for CaO the mean difference is 2.2% with a standard deviation of 1.2% (Table T5). This comparison suggests that determination of the major phases is relatively accurate; however, the consistent overestimation of calculated relative to measured SiO$_2$ possibly reflects problems in determining the abundance of biogenic silica by XRD.

Particle Size

There is an increase in the percentage of silt and fine sand-sized particles (10–100 µm) across zones of high *P*-wave velocity (Fig. F8). The volume of sediment in this moderately coarse size range compares closely with the abundance of biogenic silica (Fig. F9). Indeed, examination with a scanning electron microscope shows that bulk sediment in Sample 172-1063D-4H-4, 72–74 cm, at 26.52 mbsf, is composed of abundant and fragile sand-sized biogenic silica grains (Fig. F10). The changing particle size during sonication likely reflects destruction of biogenic silica grains. The very coarse mode at 200–400 µm evident in some samples is possibly a combination of sand-sized foraminifers and authigenic particles.

DISCUSSION

Variations in carbonate content on the Bermuda Rise can be correlated with fluctuations found in the δ^{18}O of ice in cores from Greenland (Adkins et al., 1997). Variations in grayscale at Site 1063 can be correlated similarly (Keigwin, Rio, Acton, et al., 1998). The δ^{18}O features in the Greenland ice cores have been dated (Dansgaard et al., 1993). Therefore, a preliminary time scale was assigned to the sediment interval between 25.0 and 29.5 mbsf by aligning variations in grayscale at Hole 1063D with changes in the δ^{18}O record at the Greenland Ice-core Project (GRIP) core (Fig. F11). Actual ages of the sediment were calculated by spline interpolation between control points using the software package Analyseries (Paillard et al., 1996). No time lag between the carbonate record at Site 1063 and the δ^{18}O record of the GRIP ice core was incorporated into the age model. According to this model, the carbonate abundance peaks at 25.8, 26.8, and 28 mbsf correspond to interstadials 19, 20, and 21, respectively (Dansgaard et al., 1993). Thus, as suggested by Keigwin, Rio, Acton et al., (1998), changes in sediment physical properties, especially bulk density, occur during D-O cycles.

The sediment record of D-O cycles at Site 1063 does not reflect simple fluctuations in the amount of carbonate and aluminosilicates, however. The densities of calcite and all common aluminosilicate minerals are between 2.6 and 2.8 g/cm³. Thus, even though calcite and aluminosilicate content are changing across D-O cycles, the observed density variations exceeding 0.3 g/cm³ indicate additional complexity. This complexity arises because late Quaternary sediment on the Bermuda

F6. Comparison of bulk sediment chemistry from Hole 1063D to that determined for core tops across the northwest Atlantic, p. 14.
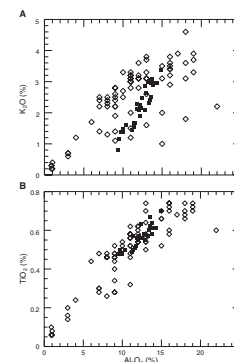
T4. Assumed chemical compositions of minerals at Site 1063, p. 23.

F7. Comparison of calcite, determined by XRD, and CaO, measured by XRF, on the same samples from Hole 1063D, p. 15.
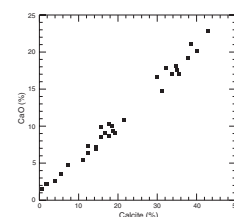
T5. Comparison of elemental abundance derived from XRD and determined by XRF, p. 24.

F8. Physical properties and particle size measurements across a short section of the study interval, p. 16.

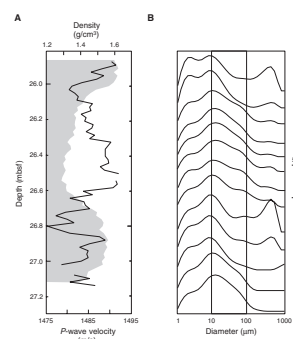Rise is a three-component system comprised of calcite, aluminosilicate minerals, and biogenic silica, and the relative abundance of all three phases varies between stadials and interstadials. Moreover, the relative abundance of various aluminosilicate minerals is also changing across D-O cycles.

The calcite fraction of Bermuda Rise sediment is mostly comprised of tests of foraminifers and coccolithophorids. Theoretically, the fluctuations in calcite could arise from increased terrigenous dilution or enhanced calcite dissolution. Keigwin and Jones (1994) suggested that terrigenous dilution is the major control on the formation of D-O cycles in Bermuda Rise sediment, although they acknowledged some dissolution during isotope Stage 4. The work presented here does not address this issue directly.

The aluminosilicate mineralogy at Site 1063 is comprised of large quantities of illite with subordinate amounts of kaolinite, chlorite, and muscovite. This result is consistent with findings of previous workers in the western North Atlantic (Ericson et al., 1961; Laine and Hollister, 1981; Keigwin and Jones, 1989). Most of the aluminosilicate minerals probably originate in eastern Canada (e.g., Laine and Hollister, 1981). However, the elemental ratios determined here suggest subtle changes in the aluminosilicate composition over D-O cycles, independent of dilution by carbonate and biogenic silica. In particular, there is an increase in the K_2O/Al_2O_3 ratio during stadials (Fig. **F5F**). This increase is possibly caused by an increase in the muscovite/illite ratio.

Silva et al. (1976) and Baker (1986) have suggested that low bulk density in glacial-age sediments reflects abundant sand-sized biogenic silica. The reason is that biogenic silica lowers grain density and increases sediment porosity (and thus water content). Such an interpretation is consistent with results presented here for Site 1063.

High concentrations of sand-sized biogenic silica might also be expected to result in a high *P*-wave velocity (e.g., Hamilton and Bachman, 1982). The reason is that coarse, angular grains in contact form a rigid framework conducive to the transmission of sound waves. The correspondence of biogenic silica and *P*-wave velocity is consistent with this interpretation. Thus, D-O cycles on the Bermuda Rise are partly the result of fluctuations in biogenic silica. The combination of low density and high compressional-wave velocity has been attributed to the presence of abundant biogenic silica by other workers (e.g., Weber et al., 1997).

CONCLUSIONS

Variations in bulk density and *P*-wave velocity occur in sediment over sub-Milankovitch (D-O) cycles on the Bermuda Rise. In an interval between 65 and 95 ka, these physical properties variations are related to changes in the relative abundance of three major components: calcite, aluminosilicate minerals, and biogenic silica. Calcite, derived from planktonic organisms, is most abundant during interstadials. Conversely, aluminosilicate minerals, transported from elsewhere in the North Atlantic, are most abundant during stadials. However, the ratio of muscovite to illite-type clays is greatest during interstadials, suggesting the source of aluminosilicate minerals changes over D-O cycles. Biogenic silica, perhaps in part derived from coastal regions (D. Winter, pers. comm., 1999), is generally more abundant during stadials, although concentrations are highly variable from one D-O cycle to an-

F9. Comparison of the biogenic silica content and the volume of sediment between 10 and 100 µm in bulk sediment, p. 17.
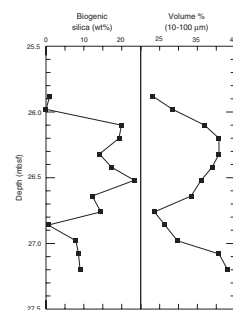
F10. Scanning electron micrograph of sediment in the >63-µm fraction of Sample 172-1063D-4H-4, 72–74 cm, p. 18.
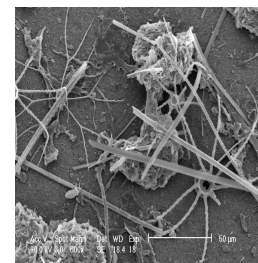
F11. A preliminary age model for the studied interval determined by comparing the grayscale record at Site 1063 to the δ18O record of ice from the well-dated Greenland Ice-core Project (GRIP) core, p. 19.
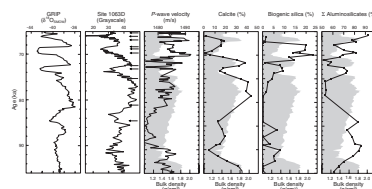
other. High concentrations of biogenic silica increase the volume of silt- and fine sand-sized sediment. Variable mixtures of all three components generate the distinctive variations in physical properties records at Site 1063: high *P*-wave velocity and high bulk density are characterized by high concentrations of calcite; low *P*-wave velocity and low bulk density are characterized by high concentrations of aluminosilicate minerals; high *P*-wave velocity and low bulk density are characterized by high concentrations of biogenic silica. The physical nature of D-O cycles on the Bermuda Rise thus reflects high-frequency changes in the accumulation of three different components.

ACKNOWLEDGMENTS

REFERENCES

Adkins, J., Boyle, E.A., Keigwin, L.D., and Cortijo, E., 1997. Variability of the North Atlantic thermohaline circulation during the last interglacial period. *Nature,* 390:154–156.

Baker, M.J., 1986. Sedimentation of the Northern Bermuda Rise [Master of Sci. thesis]. Univ. of Rhode Island, Narragansett, RI.

Barranco, F.T., Jr., Balsam, W.L., and Deaton, B.C., 1989. Quantitative reassessment of brick red lutites: evidence from reflectance spectrophotometry. *Mar. Geol.,* 89:299–314.

Biscaye, P.E., and Eittreim, S.L., 1977. Suspended particulate loads and transports in the nepheloid layer of the abyssal Atlantic Ocean. *Mar. Geol.,* 23:155–172.

Bond, G., Broecker, W., Johnsen, S., McManus, J., Labeyrie, L., Jouzel, J., and Bonani, G., 1993. Correlations between climate records from the North Atlantic sediments and Greenland ice. *Nature,* 365:143–147.

Dansgaard, W., Johnsen, S.J., Clausen, H.B., Dahl-Jensen, D., Gundestrup, N.S., Hammer, C.U., Hvidberg, C.S., Steffensen, J.P., Sveinbjörnsdottir, A.E., Jouzel, J., and Bond, G., 1993. Evidence for general instability of past climate from a 250-kyr ice-core record. *Nature,* 364:218–220.

Ericson, D.B., Ewing, M., Wollin, G., and Heezen, B.C., 1961. Atlantic deep-sea sediment cores. *Geol. Soc. Am. Bull.,* 72:193–286.

Gladney, E.S., Jones, E.A., Nickell, E.J., and Roelandts, I., 1992. 1988 compilation of elemental concentration data for USGS AGV-1, GSP-1, and G-2. *Geostand. Newsl.,* 16:111–300.

Hamilton, E.L., and Bachman, R.T., 1982. Sound velocity and related properties of marine sediments. *J. Acoust. Soc. Am.,* 72:1891–1904.

Keigwin, L.D., and Jones, G.A., 1989. Glacial-Holocene stratigraphy, chronology, and paleoceanographic observations on some North Atlantic sediment drifts. *Deep-Sea Res.,* 36:845–867.

————, 1994. Western North Atlantic evidence for millennial-scale changes in ocean circulation and climate. *J. Geophys. Res.,* 99:12397–12410.

Keigwin, L.D., Rio, D., Acton, G.D., et al., 1998. *Proc. ODP, Init. Repts.,* 172: College Station, TX (Ocean Drilling Program).

Laine, E.P., and Hollister, C.D., 1981. Geological effects of the Gulf Stream system on the northern Bermuda Rise. *Mar. Geol.,* 39:277–310.

Paillard, D., Labeyrie, L., and. Yiou, P., 1996. Macintosh program performs time-series analysis. *Eos,* 77:379.

Silva, A.J., Hollister, C.D., Laine, E.P., and Beverly, B., 1976. Geotechnical properties of the Northern Bermuda Rise. *Mar. Geotechnol.,* 1:195–232.

Taylor, J.C., 1991. Computer programs for standardless quantitative analysis of minerals using the full powder diffraction profile. *Powder Diffraction,* 6:2–9.

Weber, M.E., Niessen, F., Kuhn, G., and Wiedicke, M., 1997. Calibration and application of marine sedimentary physical properties using a multi-sensor core logger. *Mar. Geol.,* 136:151–172.

Woolfe, K.J., Fielding, C.R., Howe, J.A., Lavelle, M., and Lally, J.H., 1998. Laser-derived particle size characterization of CRP-1, McMurdo Sound, Antarctica. *Terra Antart.,* 5:383–391.

Figure F1. Location of Site 1063 on the Bermuda Rise in the northwest Atlantic Ocean.
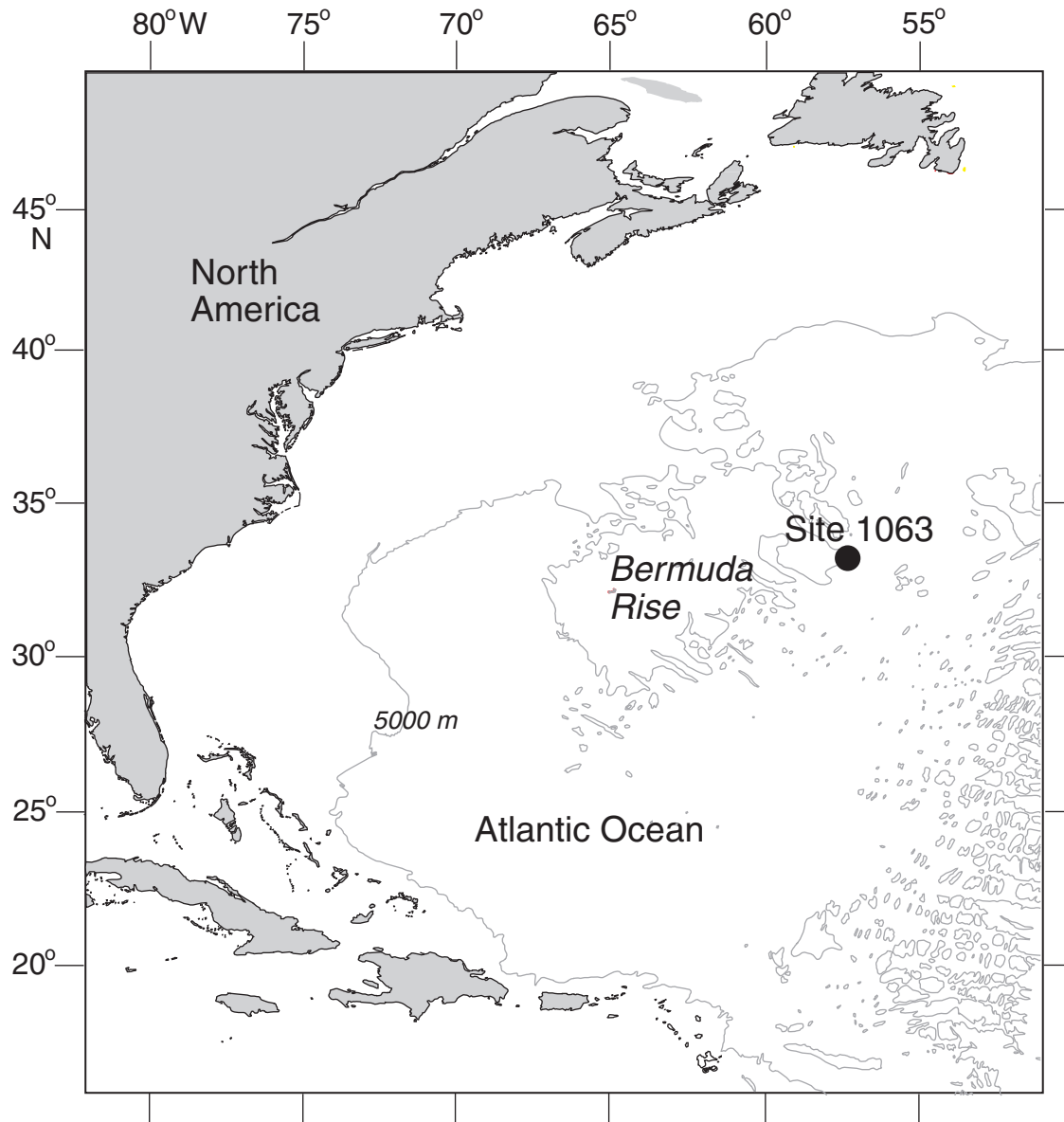
Figure F2. Physical properties records at Hole 1063D. **A.** A long portion of the hole with the study interval between the dashed lines. This interval, corresponding to the transition between glacial Stage 4 and interglacial Stage 5, was chosen because of obvious Dansgaard-Oeschger (D-O) cycles (interstadial periods are shaded areas). **B.** Expanded view of the study interval showing phase relationships between *P*-wave velocity (black line) and bulk density (shaded area).
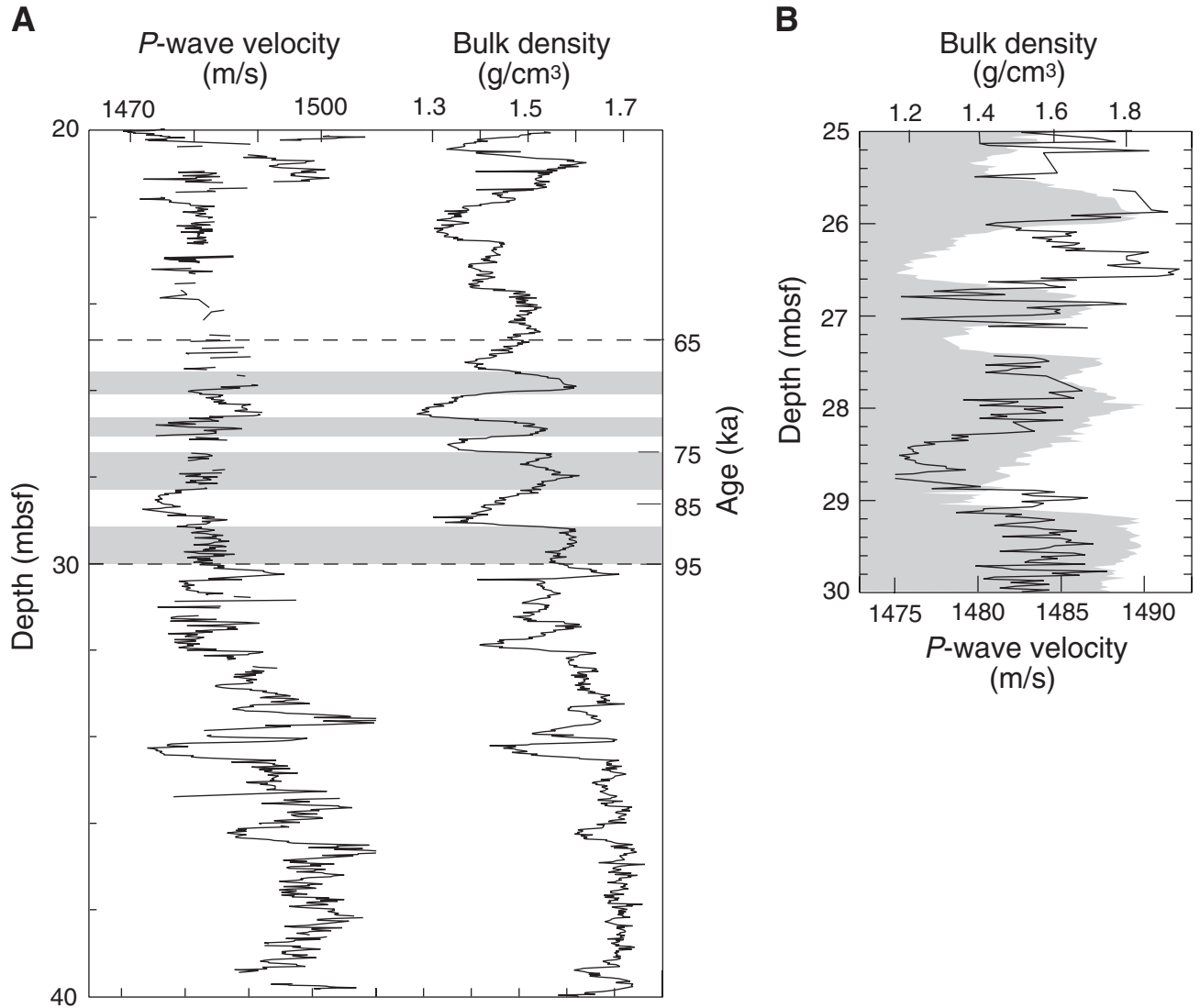
Figure F3. Repeated particle size analyses of bulk Sample 172-1063D-4H-4, 83–85 cm, during increasing sonication duration (arrows). Note the decrease in volume percent in the 10- to 200-µm size fraction. The sample was initially disaggregated by gentle agitation and then by ultrasonic means. The change in size probably reflects destruction of biogenic silica grains during sonication.
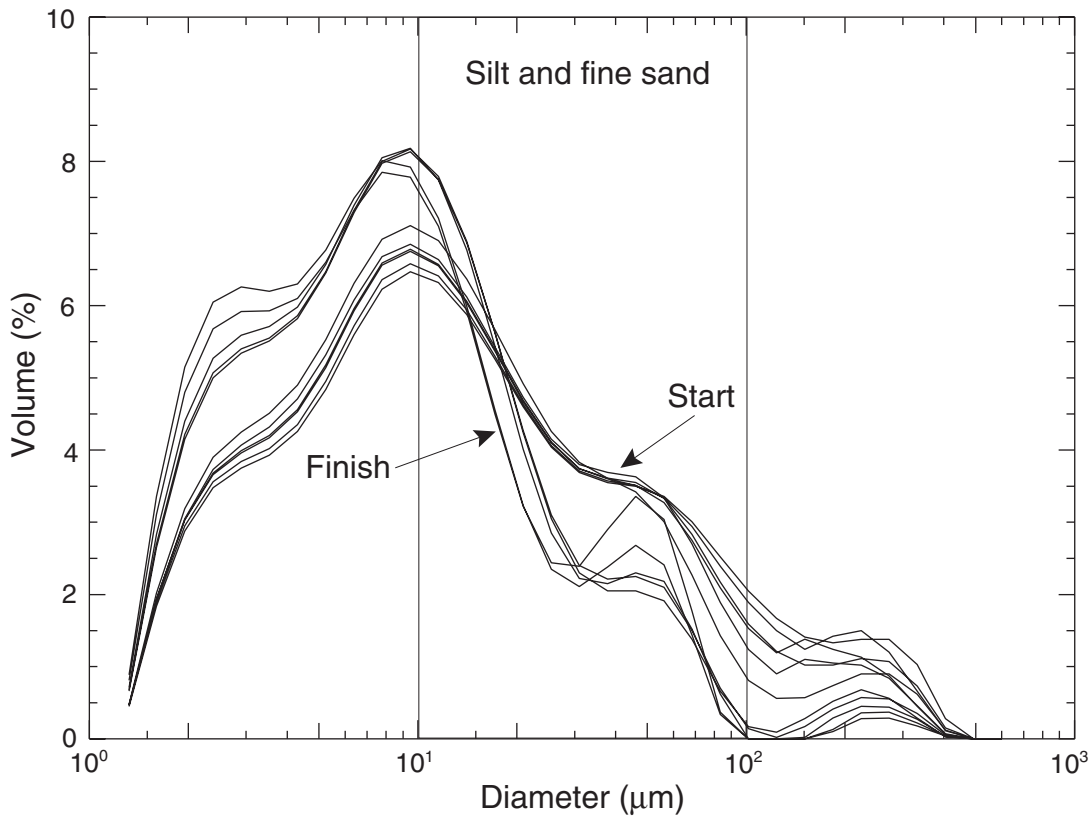
Figure F4. Reproducibility of particle size analysis on different sample aliquots after gentle agitation without ultrasound. **A.** Sample 172-1063D-4H-4, 6–8 cm. **B.** Sample 172-1063D-4H-4, 72–74 cm.
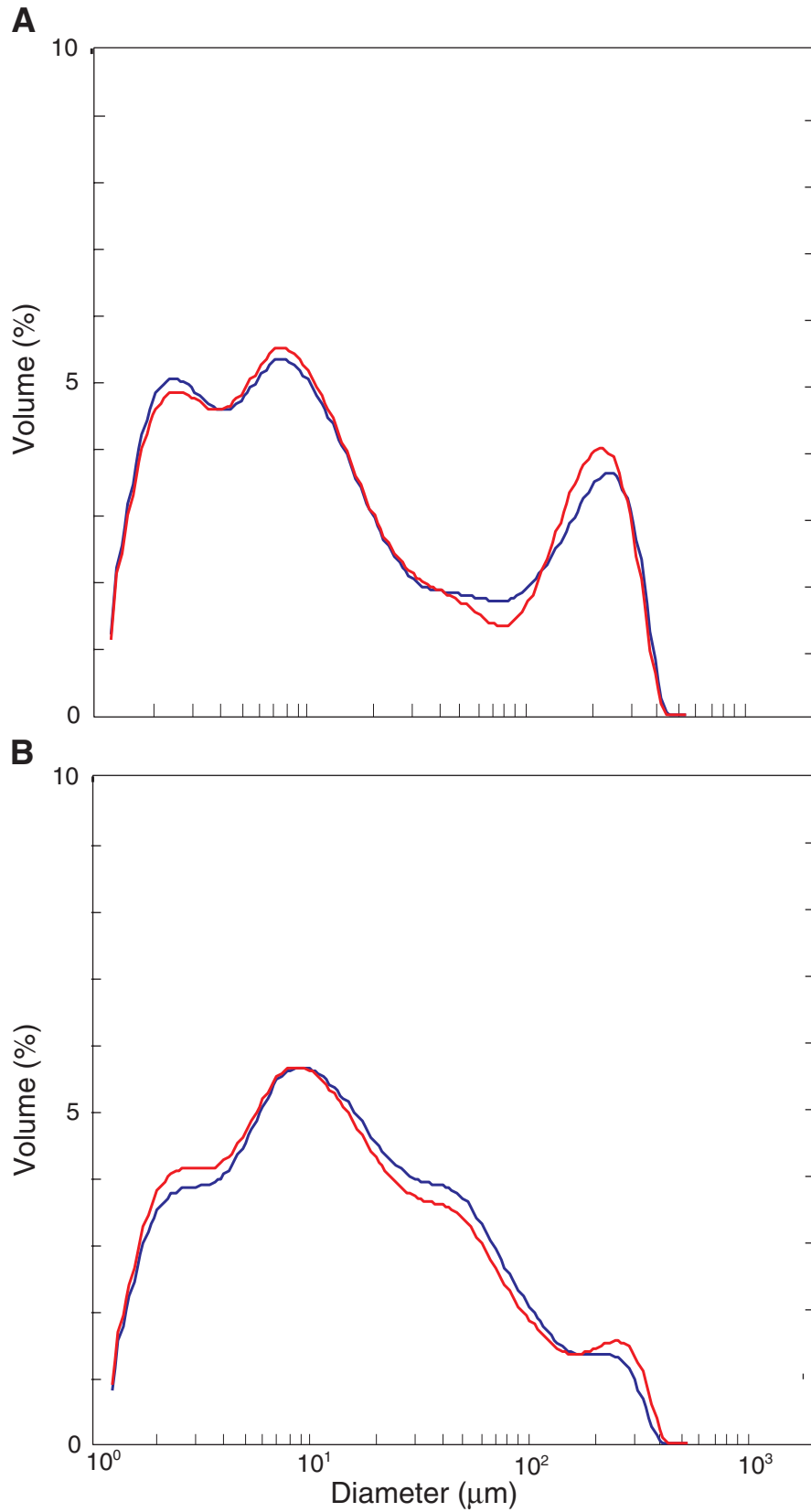
Figure F5. Downcore trends in mineralogy and chemistry compared to bulk density (shaded areas). **A.** Calcite. **B.** Total aluminosilicates (bulk sample less calcite, dolomite, and biogenic silica). **C.** Biogenic silica. **D.** SiO_2/Al_2O_3. **E.** Al_2O_3/TiO_2 (note reversed scale). **F.** K_2O/Al_2O_3. **G.** Muscovite. * = muscovite has been normalized to exclude dilution by calcite and biogenic silica.
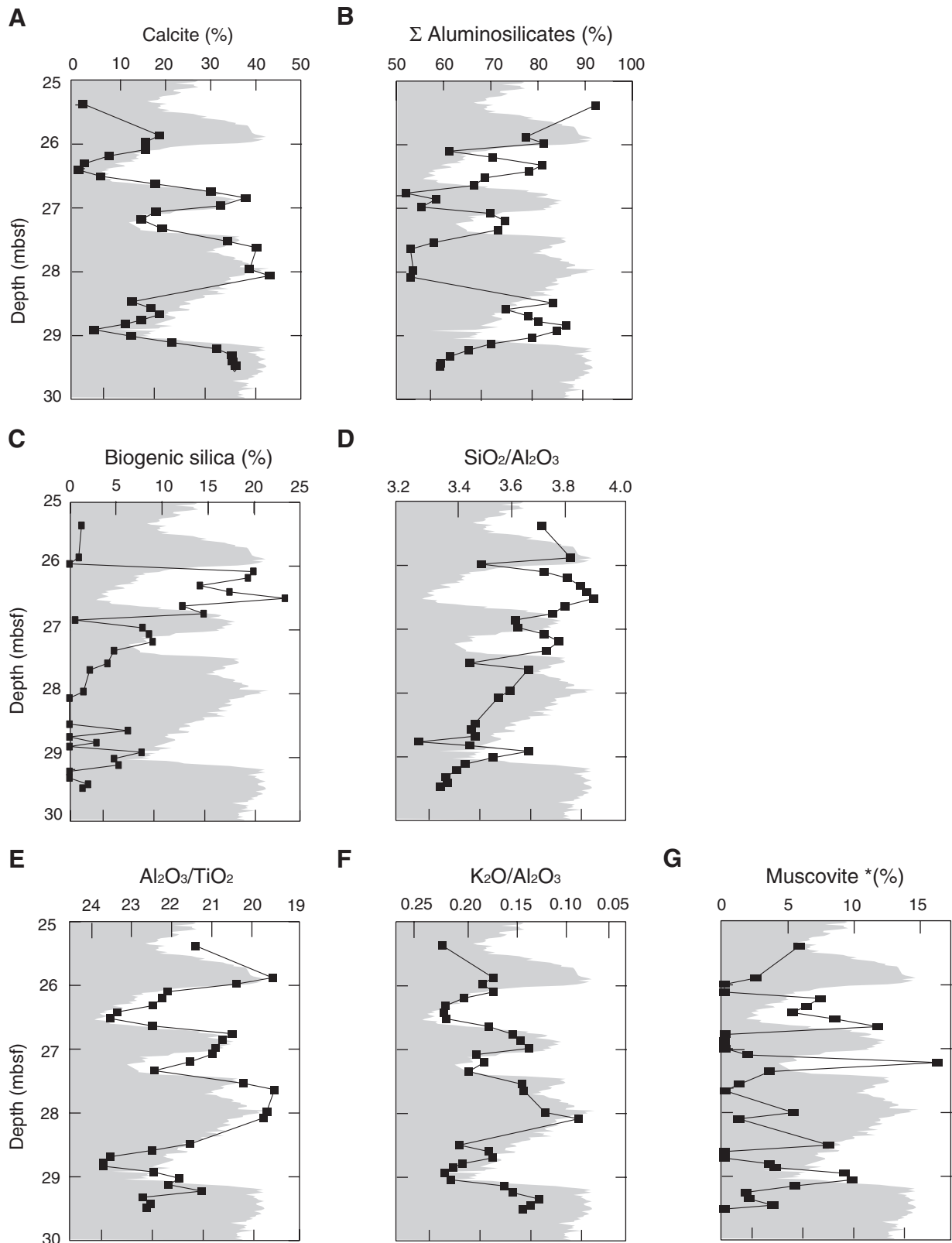
Figure F6. Comparison of bulk sediment chemistry from Hole 1063D (solid squares) to that determined for core tops across the northwest Atlantic (open diamonds). **A.** K_2O/Al_2O_3. **B.** Al_2O_3/TiO_2. Core top data are from Ericson et al. (1961).
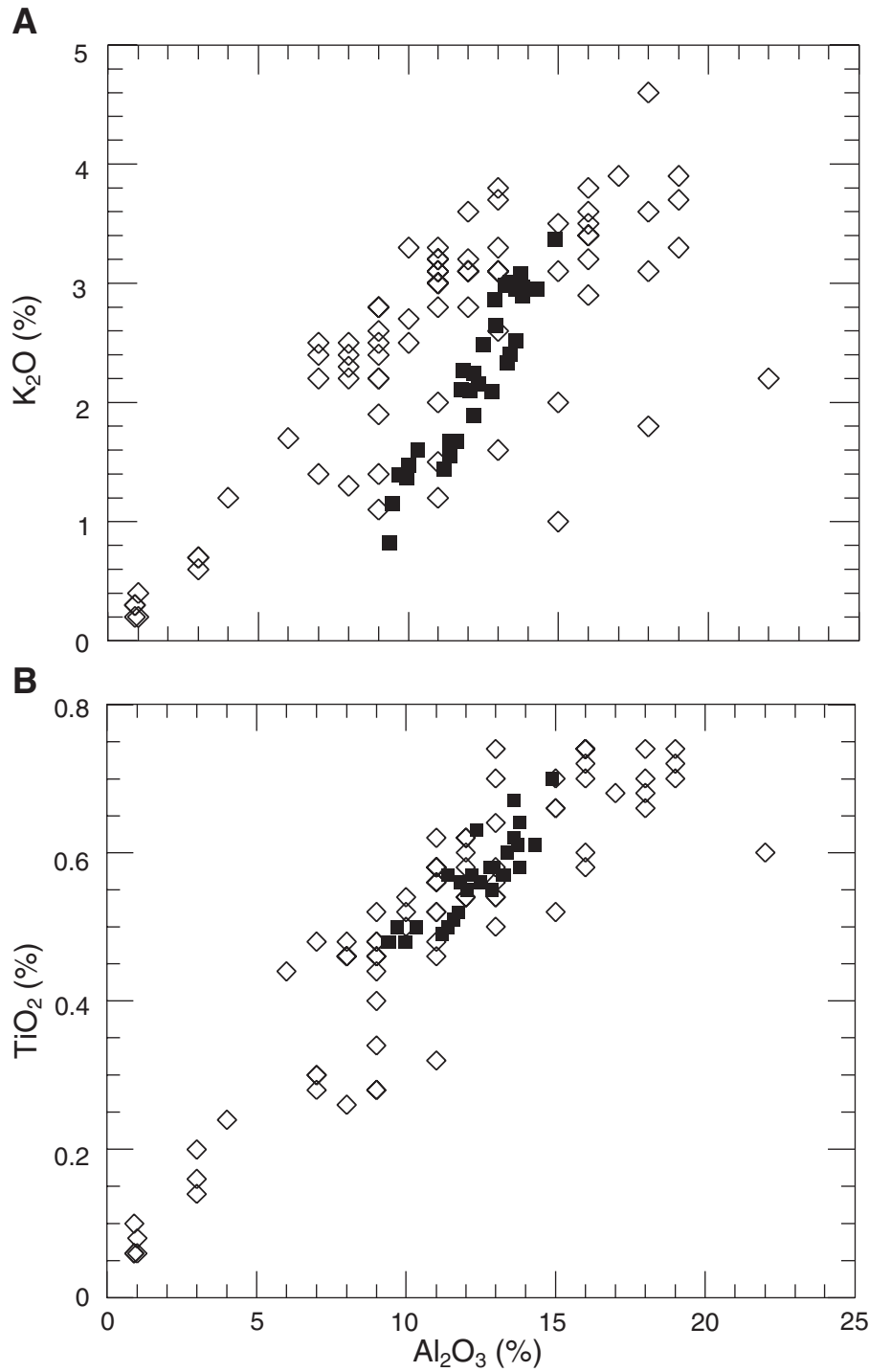
Figure F7. Comparison of calcite, determined by XRD, and CaO, measured by XRF, on the same samples from Hole 1063D. Calcium is hosted almost entirely in calcite.
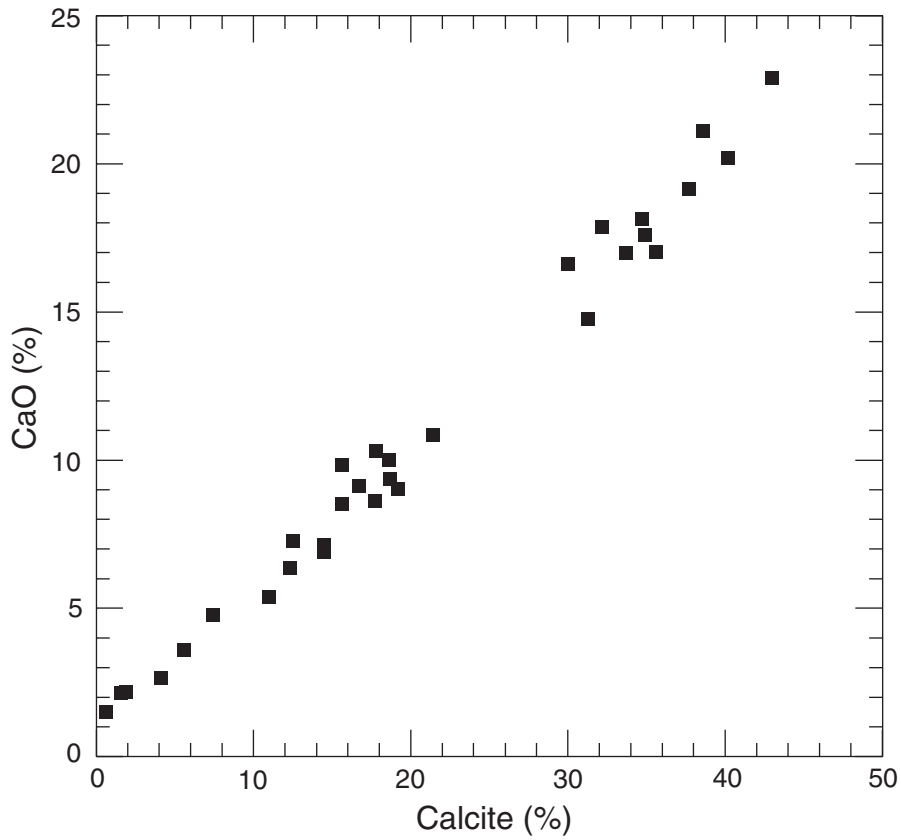
Figure F8. Physical properties and particle size measurements across a short section of the study interval. **A.** *P*-wave velocity (solid line) and bulk density (shaded area) showing a zone of high velocity and low density between 26.2 and 26.6 mbsf. **B.** Particle size analyses of bulk sediment showing an increase in the volume of silt and fine sand-sized (10–200 µm) material across the zone of high *P*-wave velocity. The vertical scale bar is in frequency percent by volume.
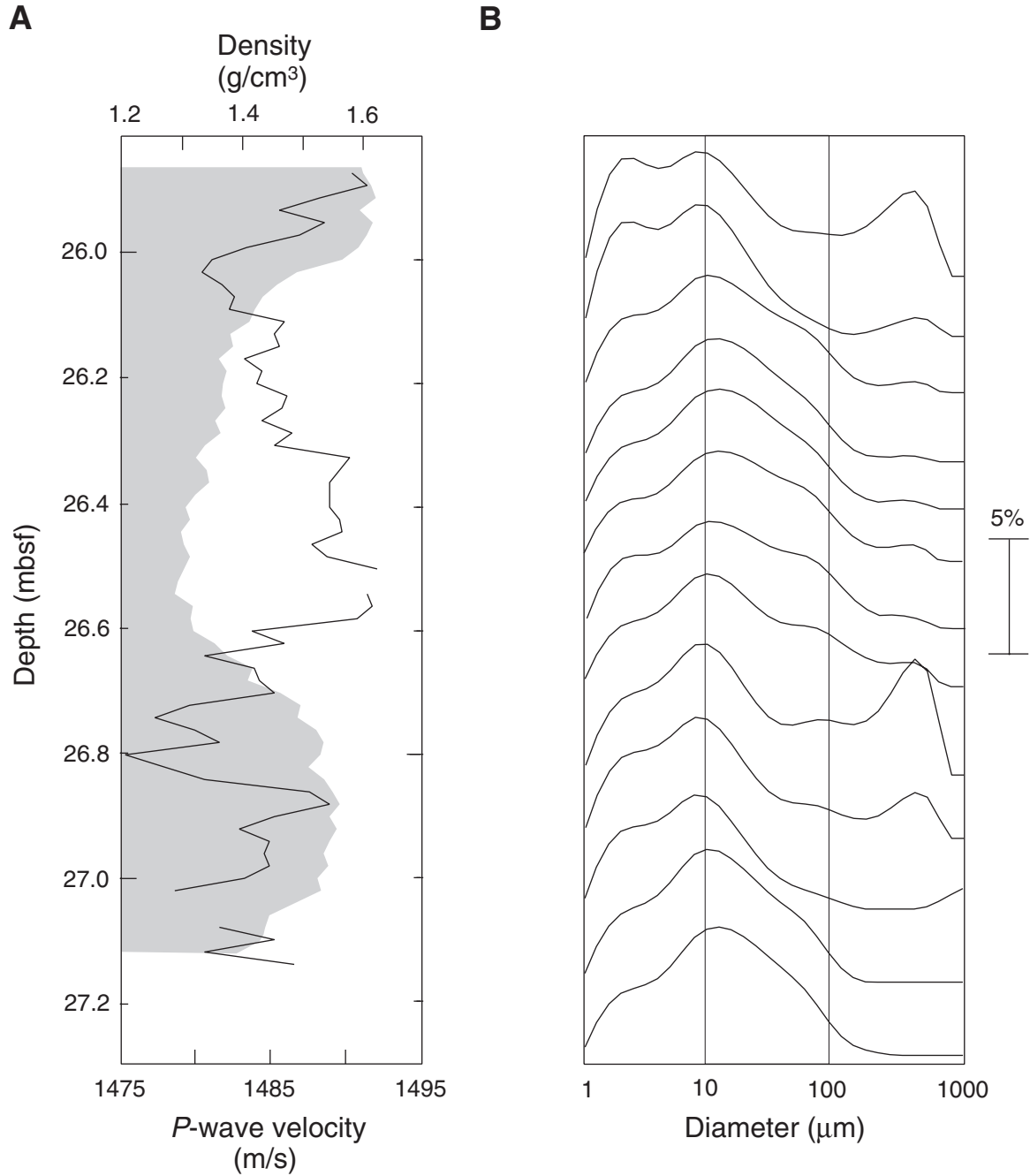
Figure F9. Comparison of the biogenic silica content (determined by XRD) and the volume of sediment between 10 and 100 μm in bulk sediment (from particle size analyses). The high degree of correlation suggests that much of the moderately coarse material is biogenic silica.
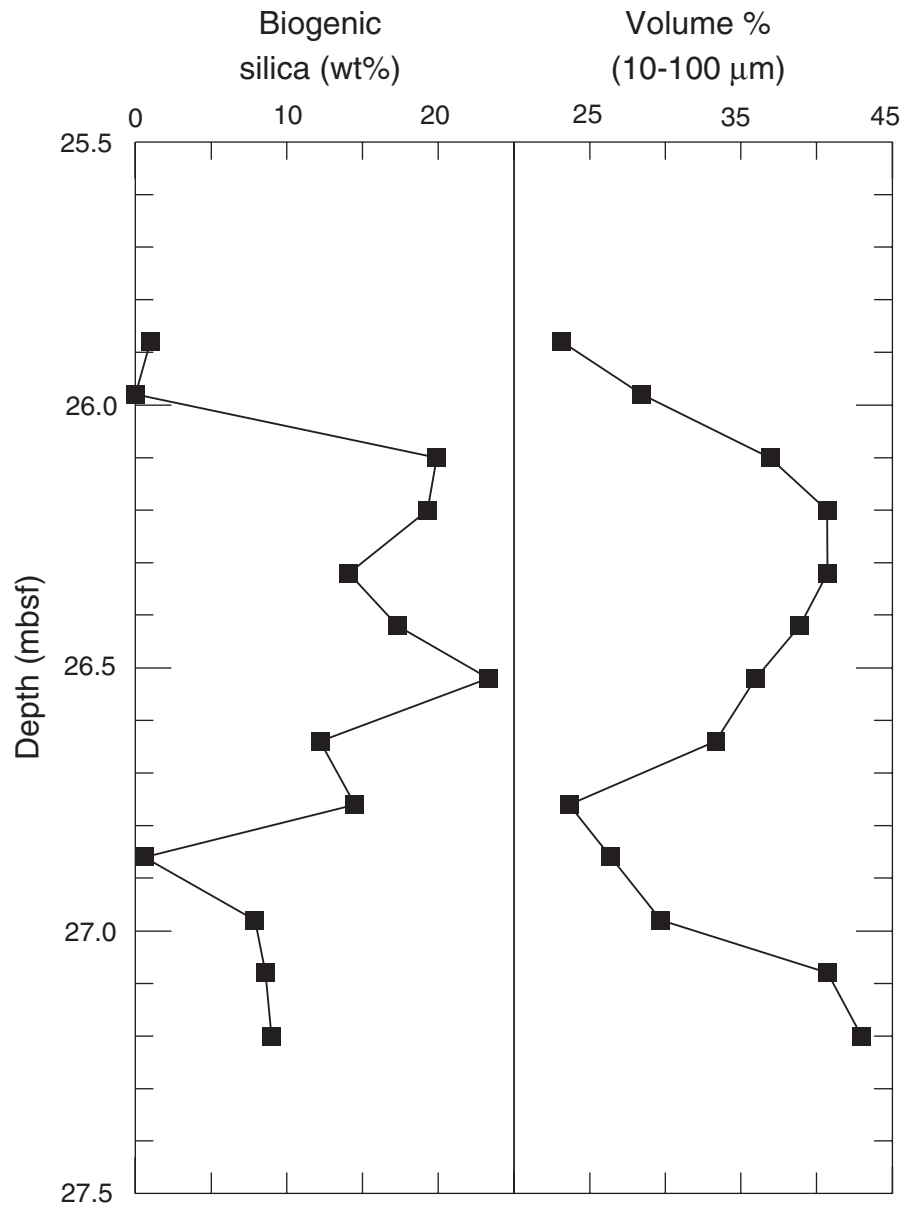
Figure F10. Scanning electron micrograph of sediment in the >63-μm fraction of Sample 172-1063D-4H-4, 72–74 cm. Note the fragile biogenic silica fragments (mainly *Bacteriostrium hyalinum*) and clay mineral-silica aggregates. The sample was wet sieved at 63 μm directly after particle size analysis.
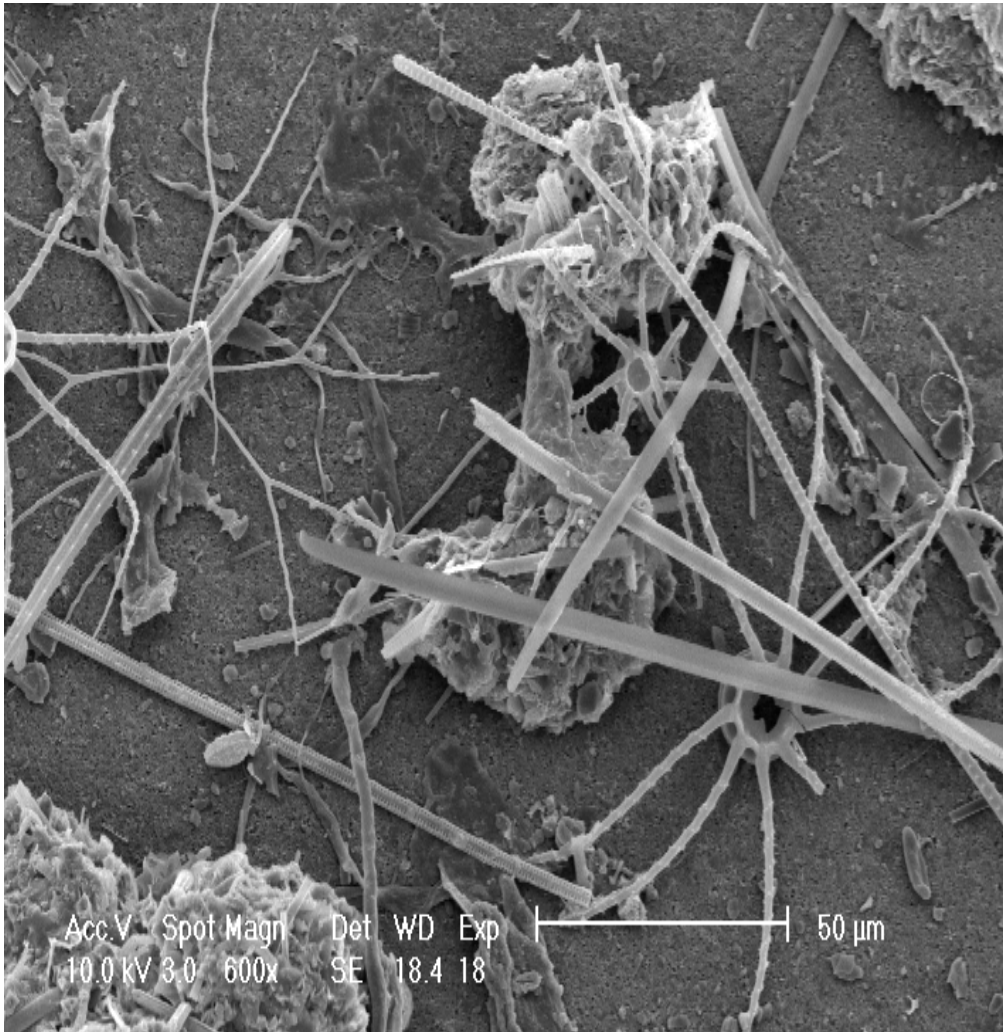
Figure F11. A preliminary age model for the studied interval determined by comparing the grayscale record at Site 1063 to the $\delta^{18}O$ record of ice from the well-dated Greenland Ice-core Project (GRIP) core. Alignment of the grayscale record was made using Analyseries (Paillard et al., 1996) based on 12 tie points (11 are marked by arrows). The tie point at 102 ka is not shown. SMOW = standard mean ocean water. Also shown is the variation in *P*-wave velocity and major sediment components over time with respect to bulk density (shaded areas).
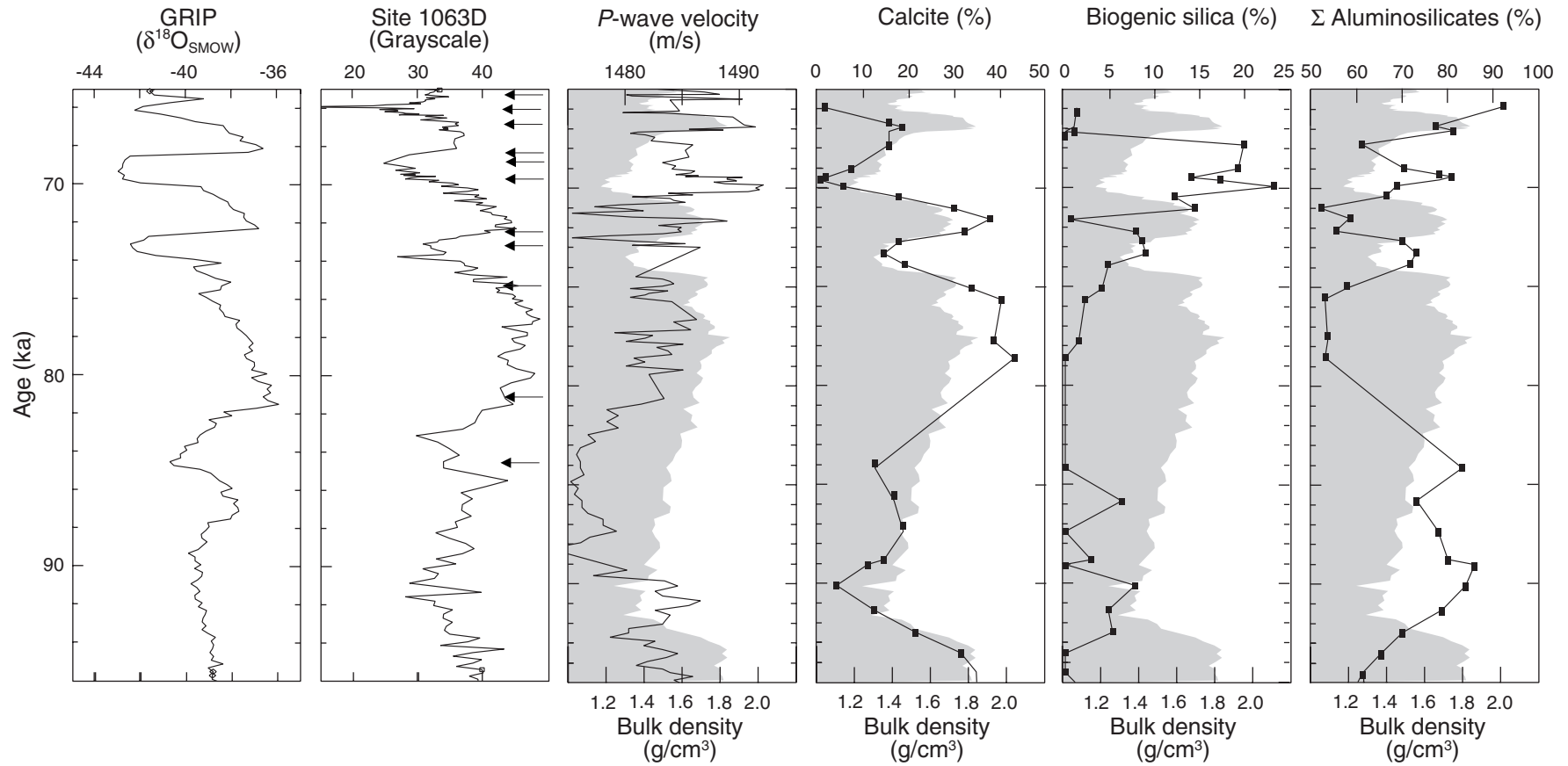
Table T1. Known and measured content of quartz-silica mixtures.

Biogenic silica (wt%)	
Known	Measured
49	36
19	17
12	7
6	6

Notes: Known biogenic silica is represented by chromatography grade silica gel. Measured biogenic silica was determined by X-ray diffraction (see "X-Ray Diffraction," p. 2, in "Methods").

Table T2. Mineralogical composition of bulk sediment from Hole 1063D determined by X-ray diffraction.

Core, section, interval (cm)	Depth (mbsf)	Age (ka)	Quartz (wt%)	Anorthite (wt%)	Halite (wt%)	Calcite (wt%)	Muscovite (wt%)	Kaolinite (wt%)	Illite-smectite (wt%)	Chlorite (wt%)	Illite (wt%)	Albite (wt%)	Orthoclase (wt%)	Hornblende (wt%)	Dolomite (wt%)	Biogenic silica (wt%)	Total
172-1063D-																	
4H-3, 108-109	25.38	66.0	25	1	2	2	6	1	5	6	13	20	9	7	3	1	100
4H-4, 7-9	25.89	66.9	25	2	0	19	2	4	5	3	15	14	6	3	3	1	100
4H-4, 17-19	25.97	67.1	20	2	1	16	0	7	7	4	20	13	7	3	3	0	100
4H-4, 28-30	26.10	67.8	12	1	1	16	0	2	9	2	11	13	7	4	2	20	100
4H-4, 39-41	26.21	69.9	16	1	1	7	5	3	7	2	10	15	7	4	2	19	100
4H-4, 50-52	26.32	69.5	18	2	1	2	5	3	11	2	11	16	8	6	2	14	100
4H-4, 61-63	26.43	69.6	19	2	1	1	4	4	10	2	11	15	7	5	3	17	100
4H-4, 71-73	26.53	69.9	19	1	1	6	6	3	6	2	7	13	7	5	1	23	100
4H-4, 83-85	26.65	70.4	19	1	1	18	8	2	3	1	7	14	7	3	3	12	100
4H-4, 96-98	26.78	71.0	14	2	1	30	0	3	1	2	8	11	7	4	3	15	100
4H-4, 105-107	26.87	71.6	16	1	0	38	0	3	7	2	9	12	6	5	3	1	100
4H-4, 116-118	26.98	72.2	13	1	1	32	0	3	6	2	10	12	6	4	3	8	100
4H-4, 127-129	27.09	72.7	17	2	1	18	1	3	9	2	10	14	7	5	2	9	100
4H-4, 139-141	27.21	73.3	21	1	1	15	12	3	3	1	6	14	6	5	3	9	100
4H-5, 3-4	27.34	73.9	20	0	2	19	3	1	8	5	12	12	6	4	3	5	100
4H-5, 23-24	27.54	75.1	18	0	2	34	1	1	2	5	14	11	5	2	3	4	100
4H-5, 33-34	27.64	75.6	16	1	2	40	0	2	5	2	9	11	5	3	3	2	100
4H-5, 68-69	27.99	77.7	14	1	2	39	3	1	3	2	7	12	5	4	5	2	100
4H-5, 78-79	28.09	78.6	15	1	1	43	1	1	4	4	10	11	5	1	3	0	100
4H-5, 118-119	28.49	84.0	24	4	1	13	7	3	6	6	13	14	6	2	4	0	100
4H-5, 128-129	28.59	85.8	18	4	2	17	0	2	7	6	17	12	5	3	2	6	100
4H-5, 138-139	28.69	87.0	20	3	1	19	0	2	6	7	17	13	6	4	2	0	100
4H-5, 148-149	28.79	88.8	20	3	1	15	3	1	6	8	19	12	6	2	2	3	100
4H-6, 3-4	28.84	89.1	22	5	1	11	4	3	5	8	15	14	7	5	2	0	100
4H-6, 13-14	28.94	90.1	21	4	1	4	8	1	12	5	13	13	6	2	3	8	100
4H-6, 23-24	29.04	91.3	21	3	2	12	8	1	4	7	13	13	7	3	3	5	100
4H-6, 33-34	29.14	92.5	19	3	0	21	4	1	5	6	9	13	6	5	3	5	100
4H-6, 43-44	29.24	93.5	18	3	1	31	1	2	1	6	14	12	6	3	3	0	100
4H-6, 53-54	29.34	94.5	15	3	1	35	1	1	4	5	13	10	5	4	3	0	100
4H-6, 63-64	29.44	95.4	16	5	1	35	2	1	1	4	9	13	5	3	3	2	100
4H-6, 68-69	29.49	95.9	15	4	1	36	0	1	2	6	11	13	5	4	3	1	100

Table T3. Chemical composition of the bulk sediment from Hole 1063D determined by X-ray fluorescence.

Core, section, interval (cm)	Depth (mbsf)	Age (ka)	SiO_2 (wt%)	TiO_2 (wt%)	Al_2O_3 (wt%)	Fe_2O_3T (wt%)	MnO (wt%)	MgO (wt%)	CaO (wt%)	Na_2O (wt%)	K_2O (wt%)	P_2O_5 (wt%)	S (wt%)	LOI (wt%)	Total
172-1063D-															
4H-3, 108-109	25.38	66.0	55.3	0.70	14.9	5.80	0.16	3.24	2.14	3.84	3.37	0.14	0.05	10.70	100.4
4H-4, 7-9	25.89	66.9	47.2	0.63	12.4	4.98	0.19	2.74	10.02	2.25	2.16	0.14	0.00	16.93	99.6
4H-4, 17-19	25.97	67.1	47.4	0.67	13.6	5.54	0.19	2.92	8.53	2.88	2.52	0.15	0.01	16.15	100.5
4H-4, 28-30	26.10	67.8	44.9	0.55	12.1	4.91	0.19	2.75	9.84	2.73	2.10	0.13	0.00	19.86	100.0
4H-4, 39-41	26.21	69.0	49.2	0.58	12.9	5.41	0.13	2.87	4.79	3.80	2.65	0.12	0.04	17.63	100.2
4H-4, 50-52	26.32	69.5	53.1	0.61	13.8	5.43	0.20	2.97	2.19	3.19	3.08	0.12	0.01	15.90	100.5
4H-4, 61-63	26.43	69.6	51.4	0.57	13.3	5.19	0.83	2.69	1.50	3.92	2.98	0.14	0.08	17.87	100.4
4H-4, 71-73	26.53	69.9	50.3	0.55	12.9	4.75	0.12	2.56	3.59	3.64	2.86	0.11	0.02	19.12	100.4
4H-4, 83-85	26.65	70.4	44.7	0.52	11.8	4.82	0.14	2.49	8.63	3.32	2.11	0.11	0.04	21.59	100.2
4H-4, 96-98	26.78	71.0	38.8	0.50	10.3	4.71	0.23	2.51	16.62	2.01	1.60	0.13	0.19	21.89	99.5
4H-4, 105-107	26.87	71.6	36.1	0.48	10.0	4.18	0.30	2.25	19.14	1.91	1.47	0.13	0.00	23.74	99.7
4H-4, 116-118	26.98	72.2	36.0	0.48	9.9	4.26	0.26	2.46	17.86	2.58	1.37	0.14	0.01	23.99	99.4
4H-4, 127-129	27.09	72.7	44.0	0.56	11.8	5.72	0.19	2.81	10.31	2.62	2.27	0.13	0.18	18.95	99.5
4H-4, 139-141	27.21	73.3	46.0	0.57	12.2	4.67	0.12	2.65	6.91	2.83	2.24	0.11	BD	21.82	100.2
4H-5, 3-4	27.34	73.9	46.5	0.56	12.5	4.54	0.22	2.65	9.03	3.35	2.49	0.12	0.08	18.30	100.3
4H-5, 23-24	27.54	75.1	39.4	0.57	11.4	4.73	0.20	2.72	17.0	2.45	1.67	0.14	0.07	20.10	100.5
4H-5, 33-34	27.64	75.6	35.5	0.50	9.7	4.68	0.19	2.42	20.2	2.48	1.39	0.13	0.49	21.80	99.5
4H-5, 68-69	27.99	77.7	33.9	0.48	9.4	5.01	0.30	2.91	21.1	2.51	1.15	0.14	0.43	22.20	99.5
4H-5, 78-79	28.09	78.6	33.3	0.48	9.4	4.01	0.31	2.57	22.9	2.07	0.82	0.13	0.05	24.30	100.3
4H-5, 118-119	28.49	84.0	47.9	0.64	13.8	5.80	0.13	3.18	7.29	2.73	2.89	0.13	BD	15.28	99.8
4H-5, 128-129	28.59	85.8	46.3	0.60	13.4	5.21	0.13	2.82	9.12	2.57	2.40	0.13	0.01	17.05	99.8
4H-5, 138-139	28.69	87.0	46.1	0.57	13.3	5.02	0.15	2.62	9.36	2.71	2.33	0.12	0.02	17.66	100.0
4H-5, 148-149	28.79	88.8	46.7	0.61	14.3	5.91	0.16	2.79	7.13	2.86	2.95	0.12	0.03	16.15	99.7
4H-6, 3-4	28.84	89.1	47.4	0.58	13.8	6.62	0.22	2.93	5.39	3.25	2.97	0.11	0.01	16.46	99.7
4H-6, 13-14	28.94	90.1	49.1	0.60	13.4	7.51	0.24	3.13	2.66	4.03	3.01	0.12	0.08	16.23	100.1
4H-6, 23-24	29.04	91.3	47.9	0.62	13.6	5.61	0.15	2.89	6.35	3.26	2.95	0.12	0.02	16.96	100.4
4H-6, 33-34	29.14	92.5	43.9	0.58	12.8	5.31	0.16	2.72	10.85	2.34	2.09	0.13	0.01	18.94	99.9
4H-6, 43-44	29.24	93.5	41.4	0.57	12.2	5.07	0.18	2.72	14.76	2.07	1.89	0.15	0.02	18.84	99.9
4H-6, 53-54	29.34	94.5	37.7	0.49	11.2	4.71	0.18	2.57	18.14	2.08	1.44	0.15	0.03	21.43	100.2
4H-6, 63-64	29.44	95.4	38.2	0.50	11.4	4.70	0.17	2.64	17.61	2.21	1.55	0.16	0.01	21.59	100.7
4H-6, 68-69	29.49	95.9	38.6	0.51	11.6	4.63	0.16	2.66	17.02	2.15	1.67	0.16	BD	21.11	100.3

Notes: BD = below detection. LOI = loss on ignition.

Table T4. Assumed chemical composition of minerals at Site 1063.

Mineral	Formula	Mass (g/mol)
Quartz	SiO_2	60.08
Anorthite	$CaAl_2Si_2O_8$	278.20
Halite	$NaCl$	58.43
Calcite	$CaCO_3$	100.09
Muscovite	$KAl_2(AlSi_3)O_{10}(OH)_2$	398.27
Kaolinite	$Al_2Si_2O_5(OH)_4$	258.12
Illite-smectite	$Al_{1.29} Fe_{0.335} Mg_{0.445} (Si_{3.82} Al_{0.19}) O_{10} (OH)_2 K_{0.415}$	386.90
Chlorite	$MgAlFeAlSiO_5(OH)_4$	310.19
Illite	$K_{0.40} Na_{0.40} Fe_{0.24} Mg_{0.34} Al_{1.50} (Al_{0.57} Si_{3.43} O_{10})(OH)_2$	379.25
Albite	$NaAlSi_3O_8$	262.20
Orthoclase	$KAlSi_3O_8$	278.31
Hornblende	$CaNaMg_2FeAl_2Si_6SiAlO_{22}(OH)_2$	831.04
Dolomite	$CaMg(CO_3)_2$	184.39
Opaline silica	$SiO_2 \cdot 2H_2O$	96.08

Table T5. Comparison of elemental abundance derived from X-ray diffraction and determined by X-ray fluorescence.

Core, section, interval (cm)	Depth (mbsf)	SiO$_2$ (wt%)		Al$_2$O$_3$ (wt%)		CaO (wt%)	
		XRD	XRF	XRD	XRF	XRD	XRF
172-1063D-							
4H-3, 108-109	25.38	63	55	16	15	3	2
4H-4, 7-9	25.89	55	47	13	12	12	10
4H-4, 17-19	25.97	54	47	16	14	10	9
4H-4, 28-30	26.10	53	45	11	12	10	10
4H-4, 39-41	26.21	59	49	13	13	5	5
4H-4, 50-52	26.32	63	53	15	14	2	2
4H-4, 61-63	26.43	64	51	14	13	2	1
4H-4, 71-73	26.53	62	50	12	13	4	4
4H-4, 83-85	26.65	54	45	12	12	11	9
4H-4, 96-98	26.78	45	39	9	10	18	17
4H-4, 105-107	26.87	41	36	10	10	23	19
4H-4, 116-118	26.98	42	36	10	10	20	18
4H-4, 127-129	27.09	53	44	12	12	11	10
4H-4, 139-141	27.21	56	46	14	12	9	7
4H-5, 3-4	27.34	52	47	12	12	12	9
4H-5, 23-24	27.54	42	39	10	11	20	17
4H-5, 33-34	27.64	38	36	9	10	24	20
4H-5, 68-69	27.99	37	34	10	9	24	21
4H-5, 78-79	28.09	37	33	9	9	25	23
4H-5, 118-119	28.49	56	48	16	14	9	7
4H-5, 128-129	28.59	52	46	14	13	11	9
4H-5, 138-139	28.69	51	46	15	13	12	9
4H-5, 148-149	28.79	54	47	16	14	9	7
4H-6, 3-4	28.84	56	47	17	14	8	5
4H-6, 13-14	28.94	60	49	16	13	4	3
4H-6, 23-24	29.04	54	48	15	14	8	6
4H-6, 33-34	29.14	50	44	13	13	14	11
4H-6, 43-44	29.24	43	41	12	12	19	15
4H-6, 53-54	29.34	40	38	12	11	21	18
4H-6, 63-64	29.44	41	38	11	11	22	18
4H-6, 68-69	29.49	40	39	11	12	22	17